Structural and spectroscopic study of oxyfluoride glasses and glass-ceramics using europium ion as a structural probe

2008 J. Phys.: Condens. Matter 20 145201

(http://iopscience.iop.org/0953-8984/20/14/145201)

J. Phys.: Condens. Matter **20** (2008) 145201 (7pp) doi:10.1088/0953-8984/20/14/145201

Structural and spectroscopic study of oxyfluoride glasses and glass-ceramics using europium ion as a structural probe

L A Bueno[1], A S Gouveia-Neto[1], E B da Costa[1], Y Messaddeq[2] and S J L Ribeiro[2]

[1] Laboratório de Fotônica, Departamento de Física, Universidade Federal Rural de Pernambuco, Recife 52171-900, PE, Brasil
[2] Instituto de Química, UNESP, CP 355, Araraquara 14801-970, SP, Brasil

Received 4 December 2007, in final form 7 February 2008
Published 4 March 2008
Online at stacks.iop.org/JPhysCM/20/145201

Abstract

Transparent oxyfluoride glasses and β-PbF_2 nanocrystals containing glass-ceramics were prepared with varying Eu^{3+} content (0.3, 0.4, 0.5 and 0.6%). The effect of Eu^{3+} content on the preparation of glass-ceramics was investigated. From differential scanning calorimetry, the T_x–T_g (T_x—temperature of the onset of crystallization; T_g—glass transition temperature) parameter for glasses has shown slight variation, and an exothermic peak near T_g called the ceramization temperature (T_c) has been observed. Heat treatments were performed at this temperature to obtain transparent glass-ceramics containing β-PbF_2 nanocrystals, identified by x-ray diffraction. Heat treatments for different periods of time were performed and were observed to be very important in the control of the crystal size and of the crystallization rate. Based upon the absorption spectra, the scattering level due to the presence of β-PbF_2 nanocrystals in the glass-ceramics was observed to be similar to that for the mother glasses. Detailed analysis of emission spectra and decay time measurements led to the identification of Eu^{3+} ions as the β-PbF_2 crystalline phase. Excitation spectra at 70 K show the interaction of Eu^{3+} ions with the fluorogermanate network.

1. Introduction

Rare earth ions containing oxyfluoride glasses have physical and chemical properties that make this class of materials potential candidates for applications in photonics [1]. These glasses may be used as precursors for infrared fibers or windows due to the possibility of changing their phonon energies and therefore the domain of wavelength transparency, depending upon the composition [2, 3]. Novel materials suitable for the development of solid-state frequency upconverters have attracted scientific and technological interest in the last few decades [4, 5]. Upconversion mechanisms involving concentration dependent cross-relaxation paths have been identified in Er^{3+} [6], Ho^{3+} [7], Yb^{3+}/Pr^{3+} [8], $Nd^{3+}/Tm^{3+}/Yb^{3+}$ [9], Ho^{3+}/Yb^{3+}, Tb^{3+}/Yb^{3+} [10] and $Tm^{3+}/Ho^{3+}/Yb^{3+}$ [11] for example. Concerning crystallization processes the so-called ultra-transparent glass-ceramics can be obtained by controlled crystallization heat treatment. If the crystalline phase comprises, for instance, a heavy metal fluoride, the final material has the optical properties for this class of crystals. The increase in the emission efficiency has been explained considering the lower phonon energy in the fluoride nanocrystals, which reduces the non-radiative decay rates, and shortens the interionic distance, favoring the energy transfer process [12–14]. On the other hand, Mortier *et al* presented the influence of different erbium compounds in the nucleation process of β-PbF_2 in fluorogermanate glasses [15, 16]. Then, one needs to understand the local structure around rare earth ions in oxyfluoride glasses and glass-ceramics in order to elucidate the glass crystallization process [17]. The Eu^{3+} ion has been widely used as a probe to investigate the environment around rare earth ions in different materials. The non-degenerate $^7F_0$–$^5D_0$ electronic transition can be studied by the fluorescence line narrowing (FLN) technique to analyze changes from site to site in the energy level diagram, lifetime, bandwidth, energy transfer process between optical ions, and migration of energy between ions in sites

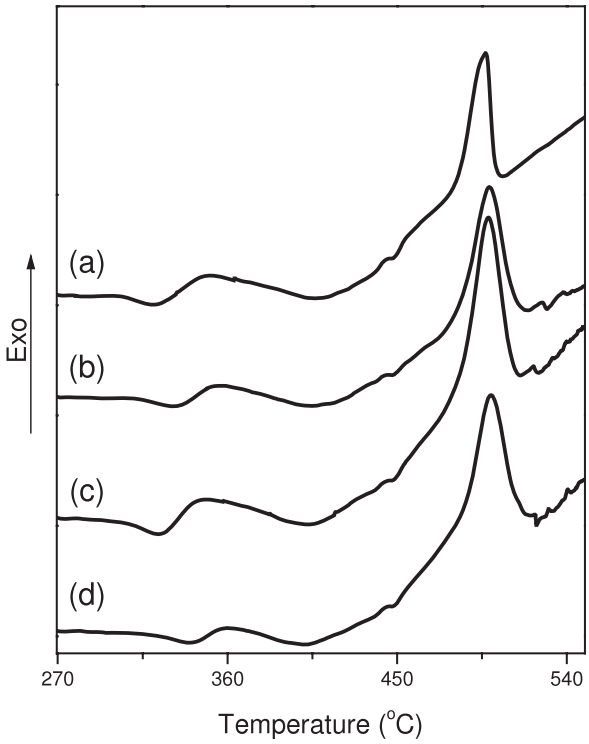

Figure 1. DSC scan for the glass (mol%) $60PbGeO_3$–$20PbF_2$–$20CdF_2$ doped with different Eu^{3+} contents (in mol%). (a) 0.3; (b) 0.4; (c) 0.5; (d) 0.6.

close in energy but spectrally different [18]. In previous papers we have reported conductivity, thermal analysis (DSC), Raman spectroscopy and NMR study of fluorogermanate glasses [19] and glass-ceramics [20]. In this work, the results on the effect of the addition of Eu^{3+} on the crystallization properties of a selected glass composition in the lead–cadmium fluorogermanate system are presented.

2. Experimental details

Glasses were prepared by melting and casting PbF_2, CdF_2 and glassy $PbGeO_3$ as described elsewhere [21–23]. Samples with composition $60PbGeO_3$–$10PbF_2$–$30CdF_2$ in mol% and with 0.3–0.6 mol% Eu^{3+} have been produced. Glass-ceramics have been obtained by heat treatments at selected temperatures based upon results from the differential scanning calorimetry (DSC) curves. Thermal analysis (differential scanning calorimetry—TA Instruments—model 3100) was performed for powdered samples in aluminum pans with heating rates of 10 °C min^{-1}. X-ray powder diffractograms were obtained with a diffractometer (D-5000 Siemens) with the Cu Kα filtered line at 0.02° s^{-1} scanning rate. Room temperature excitation and emission spectra were obtained with a spectrofluorimeter (SPEX F212I) equipped with both continuous (450 W) and pulsed (5 J/pulse; 3 μs bandwidth) Xe lamps. Spectra were all corrected for spectral variations for the lamp intensity, optics and detection system. A photomultiplier (Hamamatsu 900) was used for detection. Routine resolution of 0.5 Å has been used. UV–vis spectra, in the range 300–2500 nm, were obtained using a Cary-500 spectrophotometer with bulk and polished samples.

Table 1. Characteristic temperatures and thermal stability parameter (T_x–T_g) for glass samples doped with different Eu^{3+} contents.

[Eu^{3+}] (mol%)	T_g (°C)	T_x (°C)	T_c (°C)	T_x–T_g (°C)
0.3	305	325	350	20
0.4	309	336	355	25
0.5	306	327	347	21
0.6	320	344	361	24

3. Results and discussion

3.1. Differential scanning calorimetry analysis

Homogeneous and transparent glasses were obtained with dimensions 30 mm × 10 mm × 5 mm. Figure 1 shows DSC curves for glasses with different Eu^{3+} contents. The glass transition temperatures (T_g) and the ceramization temperatures related at the first crystallization peaks, which are observed relatively near to T_g, are presented in table 1 for samples containing 0.3, 0.4, 0.5 and 0.6 mol% Eu^{3+}. The appropriate heat treatments at 10 °C below the ceramization temperature (T_c) lead to transparent glass-ceramic formation. A second crystallization peak is observed around 773 K for all samples. Heat treatments at this temperature lead to completely crystallized samples with a mixture of fluoride and germanate crystalline phases. Rare earth ions play the role of nucleating sites for the crystallization of these glasses [14, 21, 22, 24–27]. In general, the higher the concentration of these ions the more unstable the glasses are against crystallization. Moreover, the rare earth ionic radius is also important. The smaller the ionic radius of the rare earth introduced, the more unstable are the glasses [27].

3.2. X-ray diffraction

Figures 2(a) and (b) show diffraction patterns obtained for all doped glasses and the transparent glass-ceramics obtained from them with heat treatments performed for 60 h at the temperature of the first crystallization peak (ceramization temperature—T_c). On the other hand, the selected glass sample containing 0.5 mol% of Eu^{3+} was heat treated for 2 h in order to evaluate the effect of the time of heat treatment on the crystallization process. A characteristic amorphous halo is observed for the mother glasses. Diffraction peaks that could be easily assigned to cubic β-PbF_2 are observed for the samples treated. The crystallite sizes were calculated using the Scherrer equation,

$$D = \frac{0.9\lambda}{\beta \cos\theta} \tag{1}$$

where λ is the x-ray wavelength in Å, β is the full width at half maximum of the peak and θ the diffraction angle. An XRD ratio, R, roughly evaluating the amount of crystalline phase in the glass-ceramics, was calculated with the following expression [28]:

$$R = \frac{A_1}{A_2} \tag{2}$$

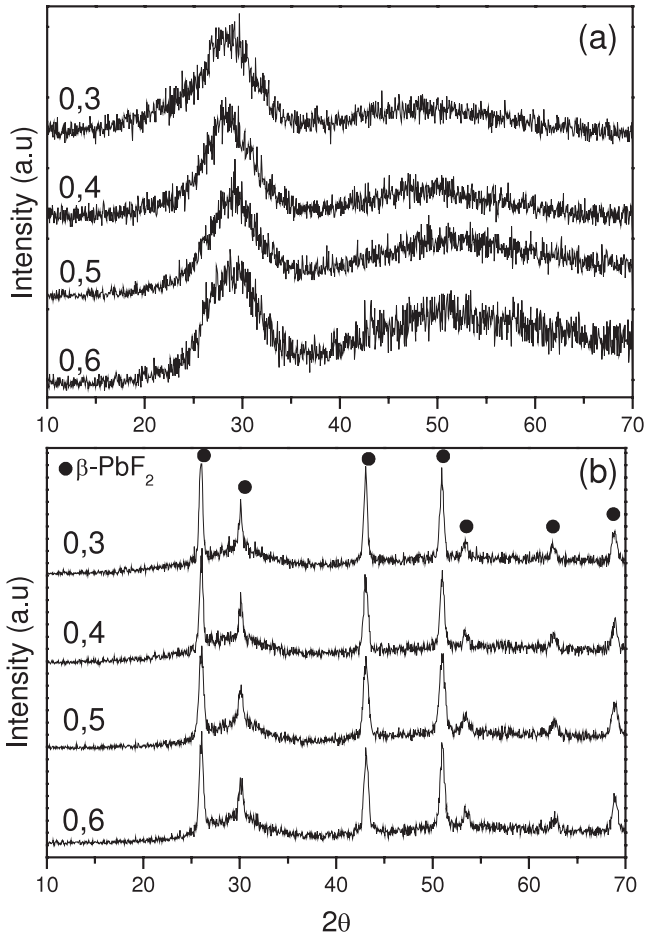

Figure 2. X-ray diffraction patterns for the (a) glass (mol%) $60PbGeO_3$–$20PbF_2$–$20CdF_2$ doped with different Eu^{3+} contents (in mol%) and (b) glass-ceramics obtained after 60 h of heat treatment.

where A_1 and A_2 are the area of the crystalline peaks and the total area of the XRD diagram, respectively, the total area corresponding to the diagram integration from $2\theta = 10°$ to $70°$. Table 2 shows these results for all glass-ceramics containing Eu^{3+} ions. No significant difference in the crystallite sizes and the amount of crystalline phase in the glass-ceramics is observed with the increase in the Eu^{3+} content. On the other hand, a mean crystallite diameter of 14 nm and 12% of crystallized fraction is obtained for the sample treated for 2 h. For the still transparent sample treated for 60 h the crystallite mean diameter amounts to 28 nm and the crystallized fraction increases to 26%. These results show that the control of the crystal size is possible in these glass-ceramics.

3.3. UV–vis analysis

An estimation of scattering properties in glasses and glass-ceramics can be made after careful analysis of absorption spectra in UV–vis. The relation of scattering level and wavelength of light allows direct comparison between glasses and glass-ceramics through the spectrum base lines. In figure 3 are shown the absorption spectra of glasses and glass-ceramic

Table 2. Crystallite sizes and the amount of crystalline phase glass-ceramic samples doped with different Eu^{3+} contents. (60 h of heat treatment.)

$[Eu^{3+}]$ (mol%)	D (nm)	F (%)
0.3	34	22
0.4	34	23
0.5	28	26
0.6	30	23

samples containing different Eu^{3+} contents. The presence of β-PbF_2 nanocrystals promotes light scattering and can be observed by base line displacement. The transparent glass and glass-ceramic scatterings follow a Rayleigh law (proportional λ^{-4}). The scattering levels for glasses and glass-ceramics are almost the same and this observation can explain very well the similarity in transparency of both materials.

3.4. Emission spectra

Figure 4 shows emission spectra obtained under 394 nm excitation for the glass and glass-ceramic samples with different Eu^{3+} contents. Transitions from the excited states ^5D_J to the lower $^7F_{J'}$ levels of the Eu^{3+} $4f^6$ configuration are observed. Inhomogeneously broadened spectra expected for glasses [29] are observed for the non-treated samples. However, the spectra become completely different in the case of transparent samples submitted to the heat treatment. The bands became structured and narrowed after heat treatment, suggesting the presence of optically active ions in crystalline phases. Additional splitting for several transitions and a decrease in the intensity of the hypersensitive $^5D_0 \rightarrow {}^7F_2$ transition around 613 nm are visible for the fully transparent sample which resulted from the heat treatment. Throughout these treatments the transparency of the samples remained unaltered. Figure 5 shows the intensity ratio of transitions $^5D_0 \rightarrow {}^7F_1$ and $^5D_0 \rightarrow {}^7F_2$. It grows with the Eu^{3+} content in both glasses and glass-ceramics. The intensity of the magnetic dipolar $^5D_0 \rightarrow {}^7F_1$ transition does not depend on the ligand field (Eu^{3+} environment). On the other hand, the electric dipolar $^5D_0 \rightarrow {}^7F_2$ transition is known to be forbidden in centrosymmetric ligand fields. Therefore one is led to conclude that decreasing in intensity for the last transition is related to an increase in the symmetry degree of the ligand field for the active ions due to the formation of cubic β-PbF_2 as shown in XRD. These modifications in the intensity ratio of transitions $^5D_0 \rightarrow {}^7F_1$ and $^5D_0 \rightarrow {}^7F_2$ would be expected for the presence of Eu^{3+} substituting the Pb^{2+} in the cubic structure of β-PbF_2, as observed in Er^{3+} doped glass and glass-ceramics in the GeO_2–PbO–PbF_2–ErF_3 system [30]. With the increase of Eu^{3+} content in the glass matrix, more ions migrate for the crystalline phase, after the glass-ceramic formation, contributing to a large increase in the intensities of transitions $^5D_0 \rightarrow {}^7F_2$. Mortier *et al* [30] report the values of the PbF_2 lattice parameter versus the local erbium content in the crystal phase. Only with a high doping level of Er^{3+} (10 mol% approximately) was it possible to observe a modification in the lattice parameter of β-PbF_2 in the glass-ceramic due the solid

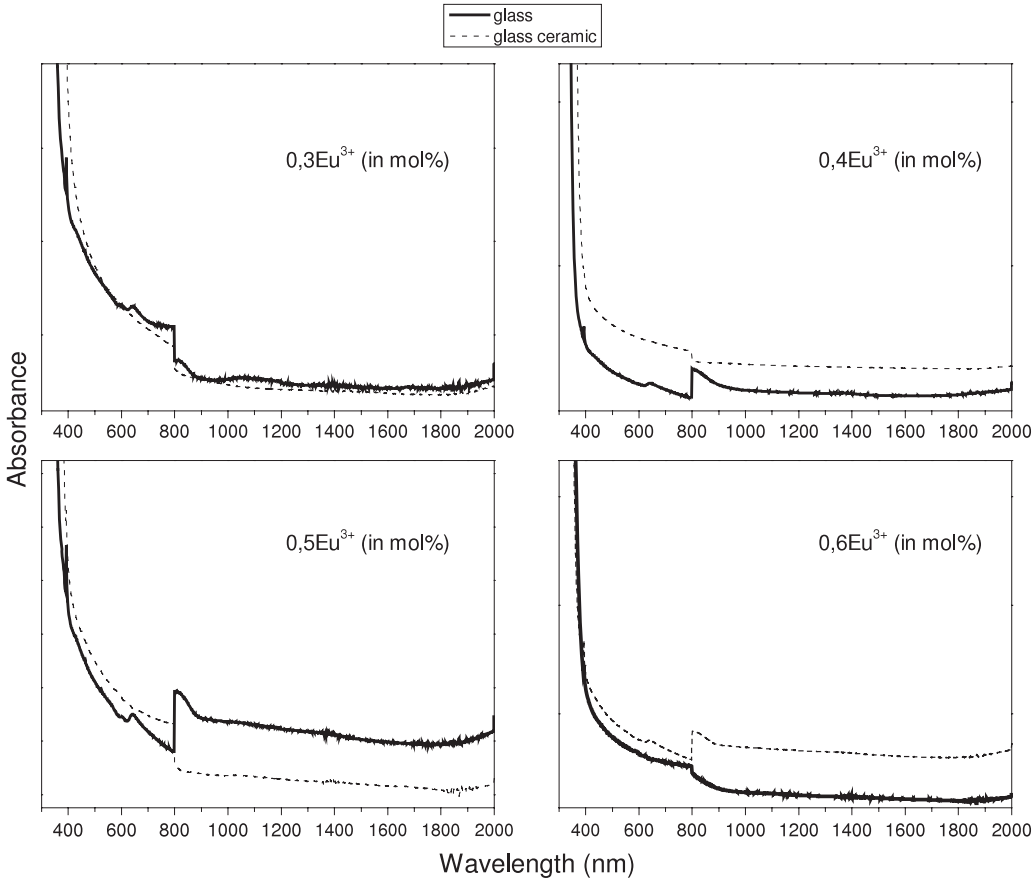

Figure 3. Absorption spectra of glasses and glass-ceramic samples containing different Eu^{3+} contents.

Table 3. The lifetime of Eu^{3+} levels is reported for samples doped with 0.5 mol% of Eu^{3+}.

Excited levels of Eu^{3+}	τ_{exp} (ms) glass	τ_{exp} (ms) glass-ceramic
$^5D_0$	3.2	3.5 and 10
$^5D_1$	1.9	2.4
$^5D_2$	0.8	1.4
$^5D_3$	0.8	0.9

solution formation ($Pb_{1-x}Er_xF_2$), observed by XRD analysis. Our XRD results for glass-ceramics are in agreement with these results because the peaks observed in figure 2(b) are attributed only to the presence of β-PbF_2 and there are no indications of formation of $Pb_{1-x}Eu_xF_2$ solid solution due to the low Eu^{3+} ion concentration.

3.5. Lifetime measurements

The experimental decay time values observed for the Eu^{3+} excited states ($^5D_0$, $^5D_1$, $^5D_2$ and $^5D_3$) provide important information to evaluate, together with emission spectra, the chemical environmental of rare earths. In table 3, decay time values for Eu^{3+} levels are reported for samples doped with 0.5 mol% of Eu^{3+}. An increase is observed for all values with the ceramization process leading to the transparent glass-ceramic, as expected on going from an oxide environment to a heavy metal fluoride one. It is possible to observe that for the level $^5D_0$ there are two lifetimes which indicate the presence of two Eu^{3+} ion sites, i.e. a vitreous environment (smaller lifetime) and a crystalline environment (larger lifetime). These results are in agreement with emission spectra and XRD results.

3.6. Emission quantum efficiency

The spontaneous Einstein emission coefficient (A) of the $^5D_0 \rightarrow {}^7F_1$ transition is constant ($\sim$50 s^{-1}) due to the weak dependence of the transition compared to the ligand field. This coefficient is related to the area under the peak of transition in the emission spectrum and the formula is

$$(\text{Transition area})_{0-J} = Ah\nu \ (J = 1, 2, 3, 4, 5, 6) \qquad (3)$$

where 0–J is related to the transitions $^5D_0 \rightarrow {}^7F_J$, with $J = 1, 2, 3, 4, 5$ and 6, A is the spontaneous Einstein emission coefficient of transition (0–J), h is Planck's constant and ν is the frequency of the baricenter of the analyzed transition.

The area and the frequency of the transition are obtained from the emission spectra. Using this equation it is possible to calculate the spontaneous Einstein emission coefficient for each one of the Eu^{3+} transitions. The ratio expressed below is used for this:

$$\frac{\text{área}_{0-j}}{\text{área}_{0-1}} = \frac{A_{0-J}h\nu_{0-J}}{A_{0-1}h\nu_{0-1}}. \qquad (4)$$

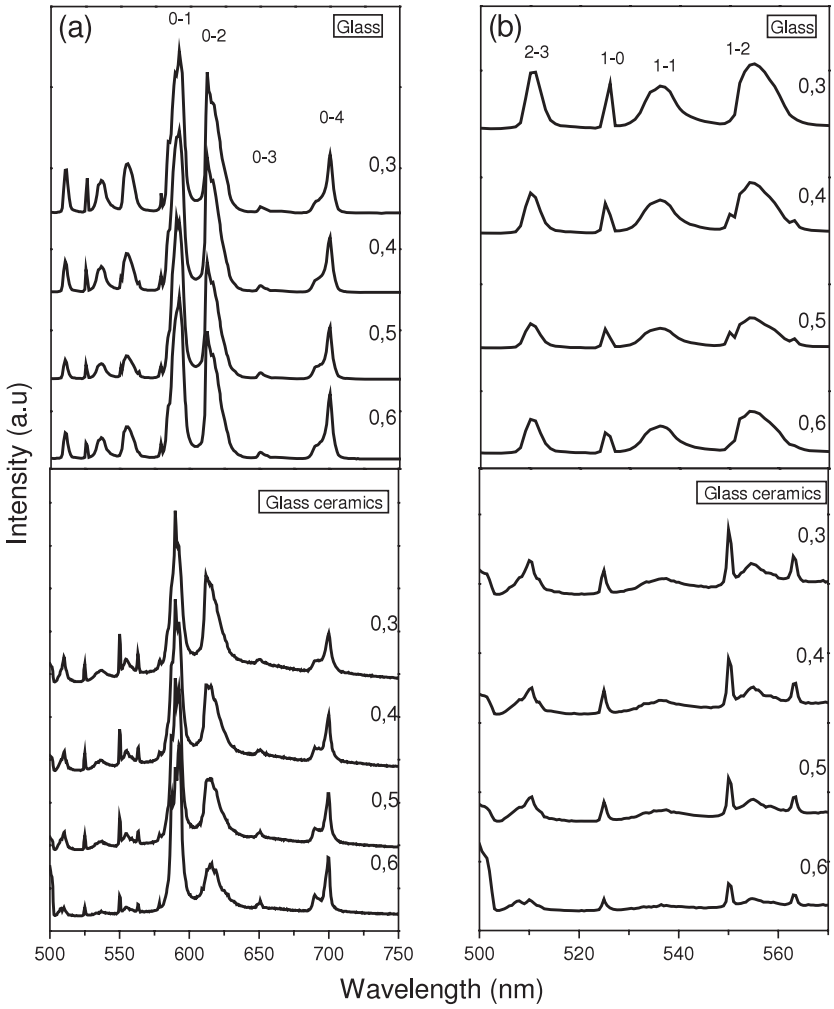

Figure 4. Emission spectra of glasses and glass-ceramic samples containing different Eu^{3+} contents. The symbols J–J' represent the transitions of the excited state ^5D_J for lower levels $^7F_{J'}$.

The sum of all spontaneous Einstein emission coefficients is the same as the constant of radioactive decay (k_{rad}) of the europium ions. When the lanthanide ions are in the excited state the return to the fundamental state can happen by two routes: radioactive (light emission) and non-radioactive (loss for heat, energy transfer etc). The inverse of the constant of radioactive decay (k_{rad}) is the same as the radioactive lifetime (τ_{rad}).

$$\tau_{rad} = \frac{1}{k_{rad}}. \tag{5}$$

The constant of experimental decay observed for a lanthanide is defined by the equation

$$k_{exp} = k_{rad} + k_{nrad} \tag{6}$$

where k_{nrad} has temperature dependent and non-dependent decay contributions. To low temperatures the dependent contributions of temperature are ignored. Then, the constant of non-radioactive decay is governed by the independent processes of the temperature. The constants k_{exp} and k_{rad} are also used to calculate the quantum efficiency (η) of emission of Eu^{3+}. The quantum efficiency (η) is a quantity that describes the number of excited particles that emit light; this quantity is expressed as

$$\eta = \frac{k_{rad}}{k_{exp}}. \tag{7}$$

Table 4. The quantum efficiency of emission (η) for the $^5D_0$ excited level for glass and glass-ceramic.

Sample	τ_{rad} (ms)	τ_{exp} (ms)	η (%)
Glass	8.5	3.2	38
Glass-ceramic	11	3.5 and 10	32 and 92

Then, we calculated the radioactive lifetimes (τ_{rad}) for the mother glass and for transparent vitroceramics doped with 0.5% of Eu^{3+} ions (in mol%). Using the results of experimental lifetimes (τ_{exp}), the quantum efficiency of emission (η) was calculated for the $^5D_0$ excited level. Table 4 shows the results. The crystallization of β-PbF_2 and consequently the transparent vitroceramic formation show an increase in the level $^5D_0$ emission efficiency. This efficiency in the glass is 38%, while for the vitroceramic, due to the existence of two lifetimes, it is 32 and 92%. The smallest

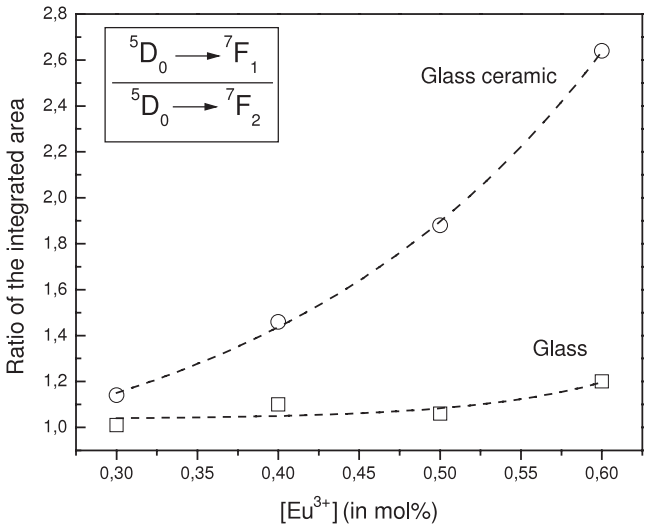

Figure 5. Variation of the intensity ratio among the $^5D_0 \rightarrow {}^7F_1$ and $^5D_0 \rightarrow {}^7F_2$ transitions $(0-1/0-2)$ as a function of the Eu^{3+} content for the glasses and transparent glass-ceramics.

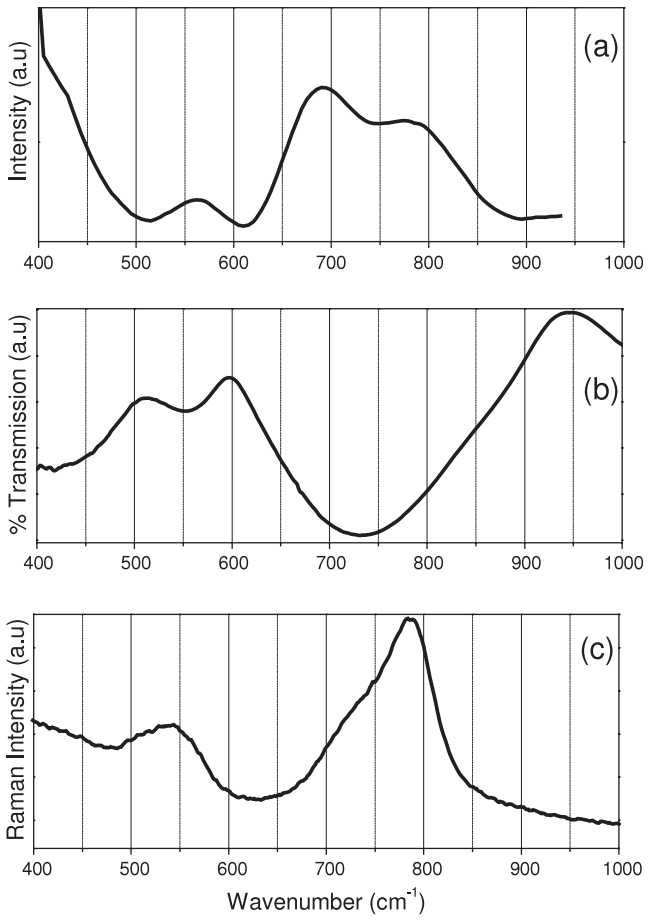

Figure 6. Glass. (a) Eu^{3+} vibronic spectrum. The $^7F_0 \rightarrow {}^5D_2$ electronic line at 21 560 cm^{-1} is taken as a reference (zero). (b) Infrared transmission spectrum. (c) Raman scattering spectrum.

efficiency value is in agreement with that obtained for the glass (38%), indicating that some Eu^{3+} ions are present in the vitreous phase of the vitroceramic. On the other hand, the

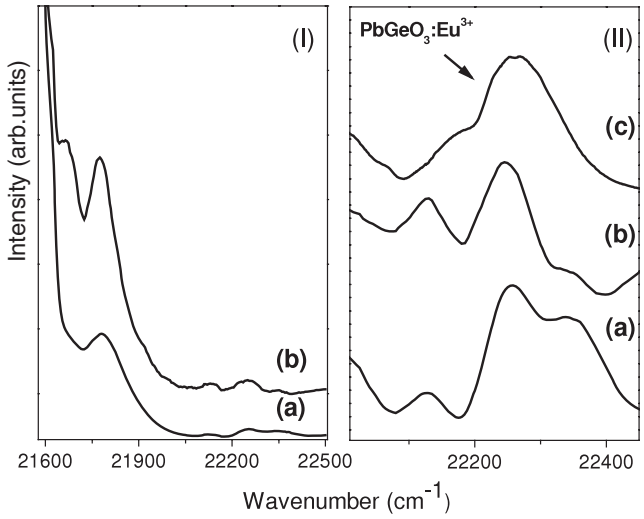

Figure 7. (I) Vibronic spectra: (a) glass; (b) transparent glass-ceramic. (II) Selected region of the vibronic spectra: (a) glass; (b) transparent glass-ceramic; (c) vibronic spectrum observed in $PbGeO_3$ [29] for comparison purposes.

largest quantum efficiency is related to the Eu^{3+} ions in the β-PbF_2 crystal phase, because the $^5D_0$ level quantum efficiency of Eu^{3+} ions in crystalline materials is, usually, around 100%.

3.7. Vibronic spectra

Figure 6(a) shows vibronic spectra obtained for the glass sample containing 0.5 mol% Eu^{3+} appearing together with the excitation band assigned to the $^7F_0 \rightarrow {}^5D_2$ Eu^{3+} transition at around 21560 cm^{-1}. Figures 6(b) and (c) show the infrared transmission spectrum and Raman scattering spectrum for the same sample. Figure 7(I) displays vibronic spectra obtained for the mother glass and the transparent glass-ceramic. Figure 7(II) shows a selected spectral region of both spectra together with the vibronic spectrum obtained for a Eu^{3+} containing lead metagermanate glass ($PbGeO_3$:Eu^{3+} (0.5 mol%)) studied before for comparison purposes [29]. Both IR active and Raman active bands appear in the vibronic spectrum. The vibronic bands corresponding to the wavenumbers of 653 and 750 cm^{-1} relate to Q^2 structures of the metagermanate chain, where Q^n is the usual nomenclature identifying the number n of bridging oxygen atoms connecting [GeO_4] tetrahedra. Bands corresponding to the wavenumbers of 562, 689 and 786 are identified in the vibronic spectrum of the fluorogermanate glass, corresponding to Q^2 structures with some substitution of fluoride ions for oxide ions in the glass network. One vibrational mode of 219 cm^{-1} is attributed to Eu^{3+} ions interacting strongly with metal fluoride rich regions. With the crystallization, vibrational modes of 94 and 201 cm^{-1} are identified and might be related to the PbF_2 crystalline phase. The vibronic spectrum still shows the interaction of Eu^{3+} with the fluorogermanate network by the observation of vibrational modes at 556, 676 and 778 cm^{-1}, and the partition of Eu^{3+} ions between the crystalline fluoride based and amorphous

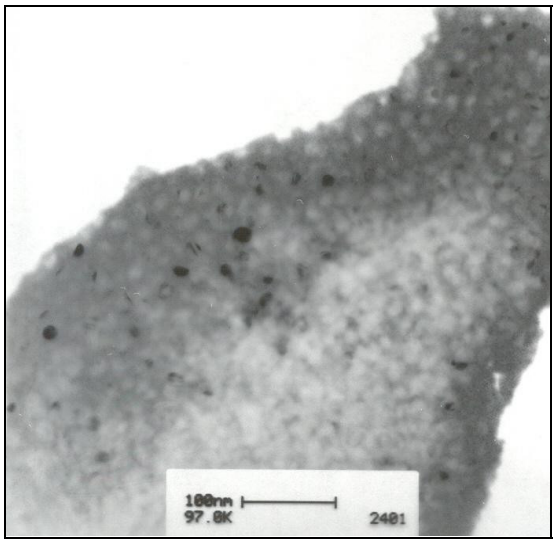

Figure 8. TEM micrography obtained for the transparent Eu^{3+} doped sample subjected to a 60 h heat treatment.

germanate based phases can therefore be studied by this spectroscopy.

3.8. Transmission electronic microscopy (TEM)

To determine the 'clusters' inside vitroceramics TEM was utilized. Figure 8 presents TEM of a vitroceramic doped with 0.5% of Eu^{3+} (in mol%). Immersed crystals in the amorphous matrix, without cluster presence and a size distribution around 30 nm, are observed.

4. Conclusion

The study involving the glass-ceramics doped with different Eu^{3+} ion contents has shown that the parameter of stability T_x–T_g for the glasses is independent of the Eu^{3+} content. The glass-ceramics presented β-PbF_2 nanocrystals dispersed in a glass matrix, with the size of crystals and the crystallized fraction depending on the time of heat treatment. Based upon the absorption spectrum study, the existence of scattering related to the presence of β-PbF_2 nanocrystals in transparent glass-ceramics was determined. However, the scattering is very similar to the glass, explaining the similar transparency of the glass-ceramics and glasses. Analyzing the emission spectra and the excited state lifetimes of Eu^{3+} ions in the glass-ceramics, it is possible to determine the presence of Eu^{3+} ions in the crystalline phase of β-PbF_2. The excitation spectra at 70 K showed various types of Eu^{3+} ion environment like Eu–F–Pb, Eu–F–Ge, Eu–O–Ge in glasses and glass-ceramics in these systems. The results of vibronic spectra show the interaction of Eu^{3+} ions with the fluorogermanate network.

Acknowledgments

The authors acknowledge FAPESP, FACEPE and CNPq (Brazilian agencies) for financial support.

References

[1] Bueno L A, Gomes A, Messaddeq Y, Santilli C, Dexpert-Ghys J and Ribeiro S J L 2005 *J. Non-Cryst. Solids* **351** 1743
[2] Varshneya A K 1993 *Fundamentals of Inorganic Glasses* (New York: Academic) (New York State College of Ceramics, Alfred University, Alfred)
[3] Doremus R H 1994 *Glass Science* (New York: Wiley)
[4] Auzel F 1973 *Proc. IEEE.* **61** 758
[5] Tanabe S, Suzuki K, Soga N and Hanada T 1995 *J. Lumin.* **65** 247
[6] Gouveia-Neto A S, da Costa E B, Bueno L A and Ribeiro S J L 2004 *J. Alloys Compounds* **375** 224
[7] Gouveia-Neto A S, da Costa E B, Bueno L A and Ribeiro S J L 2004 *J. Lumin.* **110** 79
[8] Gouveia-Neto A S, da Costa E B, Bueno L A and Ribeiro S J L 2004 *Opt. Mater.* **26** 271
[9] Gouveia-Neto A S, da Costa E B, dos Santos P V, Bueno L A and Ribeiro S J L 2003 *J. Appl. Phys.* **94** 5678
[10] Gouveia-Neto A S, Bueno L A, Afonso A C M, da Costa E B, Messaddeq Y and Ribeiro S J L 2008 *J. Non-Cryst. Solids* **354** 509
[11] Gouveia-Neto A S, Bueno L A, do Nascimento R F, da Silva E A, da Costa E B and do Nascimento V B 2007 *Appl. Phys. Lett.* **91** 1
[12] Guinhos F C, Nóbrega P C and Santa-Cruz P A 2001 *J. Alloys Compounds* **323** 358
[13] Mendez-Ramos J, Lavın V, Martın I R, Rodrıguez-Mendoza U R, Gonzalez-Almeida J A, Rodrıguez V D, Lozano-Gorrın A D and Nunez P 2001 *J. Alloys Compounds* **323/324** 753
[14] Beall G H and Pinckney L R 1999 *J. Am. Ceram. Soc.* **82** 5
[15] Mortier M, Chateau C, Genotelle M and Gardant N 2003 *J. Non-Cryst. Solids* **326/327** 287–91
[16] Mortier M 2003 *J. Non-Cryst. Solids* **318** 56
[17] Ribeiro S J L, Bueno L A, Messaddeq Y, Gouveia-Neto A S, Tambelli C C, Donoso J P, Magon C J and Dexpert-Ghys J 2006 *Mater. Sci. Forum* **514** 1299
[18] Weber M J 1986 *Laser Spectroscopy of Solids* vol 49 (Berlin: Springer) p 189
[19] Tambelli C C, Donoso J P, Magon C J, Bueno L A, Messaddeq Y, Ribeiro S J L and Oliveira L F C 2004 *J. Chem. Phys.* **120** 9638
[20] Bueno L A, Donoso J P, Magon C J, Kosacki I, Dias Filho F A, Tambelli C, Messaddeq Y and Ribeiro S J L 2005 *J. Non-Cryst. Solids* **351** 766
[21] Bueno L A, Melnikov P, Messaddeq Y and Ribeiro S J L 1999 *J. Non-Cryst. Solids* **247** 87
[22] Silva M A P, Briois V, Poulain M, Messaddeq Y and Ribeiro S J L 2003 *J. Phys. Chem. Solids* **64** 95
[23] Bueno L A, Messaddeq Y, Ribeiro S J L and Dias Filho F A 2005 *J. Non-Cryst. Solids* **351** 3804
[24] Tikhomirov V K, Furniss D, Seddon A B, Reaney I M, Beggiora M, Ferrari M, Montagna M and Rolli R 2002 *Appl. Phys. Lett.* **81** 1937
[25] Clara Goncalves M, Santos L F and Almeida R M 2002 *C. R. Chimie* **5** 845
[26] Mendez-Ramos J, Lavin V, Martin I R, Rodriguez-Mendoza U R, Rodriguez V D, Lozano-Gorrin A D and Nunez P 2003 *J. Appl. Phys.* **94** 2295
[27] Bueno L A 2003 *PhD Thesis* Instituto de Química-State University of São Paulo (UNESP) (in Portuguese)
[28] Dantelle G, Mortier M, Vivien D and Patriarche G 2005 *Chem. Mater.* **17** 2216
[29] Ribeiro S J L and Sá G F 1994 *J. Braz. Chem. Soc.* **5** 77
[30] Mortier M, Goldner P, Chateau C and Genotelle M 2001 *J. Alloys Compounds* **323/324** 245